ELSEVIER

J. Non-Newtonian Fluid Mech. 128 (2005) 172–184

Journal of Non-Newtonian Fluid Mechanics

www.elsevier.com/locate/jnnfm

Laminar transitional and turbulent flow of yield stress fluid in a pipe

J. Peixinho[a,b,*], C. Nouar[a], C. Desaubry[a], B. Théron[b]

[a] *LEMTA, Laboratoire d'Énergétique et de Mécanique Théorique et Appliquée, UMR 7563, 2, avenue de la Forêt de Haye, BP 160, 54 504 Vandœuvre-lès-Nancy Cedex, France*

[b] *Schlumberger 1, rue Becquerel, 92 140 Clamart Cedex, France*

Received 6 November 2003; received in revised form 21 March 2005; accepted 29 March 2005

Abstract

This paper presents an experimental study of the laminar, transitional and turbulent flows in a cylindrical pipe facility (5.5 m length and 30 mm inner diameter). Three fluids are used: a yield stress fluid (aqueous solution of 0.2% Carbopol), a shear thinning fluid (aqueous solution of 2% CMC) without yield stress and a Newtonian fluid (glucose syrup) as a reference fluid. Detailed rheological properties (simple shear viscosity and first normal stress difference) are presented. The flow is monitored using pressure and (laser Doppler) axial velocity measurements. The critical Reynolds numbers from which the experimental results depart from the laminar solution are determined and compared with phenomenological criteria. The results show that the yield stress contribute to stabilize the flow. Concerning the transition for a yield stress fluid it has been observed an increase of the root mean square (*rms*) of the axial velocity outside a region around the axis while it remains at a laminar level inside this region. Then, with increasing the Reynolds number, the fluctuations increase in the whole section because of the apparition of turbulent spots. The time trace of the turbulent spots are presented and compared for the different fluids. Finally, a description of the turbulent flow is presented and shows that the *rms* axial velocity profile for the Newtonian and non-Newtonian fluids are similar except in the vicinity of the wall where the turbulence intensity is larger for the non-Newtonian fluids.

1. Introduction

The present study deals with the laminar, transitional and turbulent flow of a viscoplastic fluid in a cylindrical pipe. The origin of this study comes from the oil industry, where the control of processes requires the knowledge of the flow characteristics in ducts for different flow rates. The fluids used are shear thinning and possess a yield stress, τ_Y. Their rheological behaviour is usually described by the Herschel–Bulkley model.

In laminar fully developed flow, the axial velocity profile is characterized by a plug zone around the axis of the duct moving with the maximum velocity. The radius r_p of the plug zone depends on the power law index n and the Herschel–Bulkley number Hb also called generalized Bingham number B (the ratio of the yield stress to a nominal viscous shear stress). With increasing the flow rate, the viscous forces increase, reducing the plug zone radius. The axial velocity profile is then less flat and the ratio of the plug zone velocity to the bulk velocity increases. These results are well known in the literature (Bird et al. [1]) and will be presented briefly in Section 4.

Concerning the critical Reynolds number, phenomenological criteria ([2–7]) developed in the 50's are widely used in industrial applications. A general approach is to use a dimensionless ratio of two physical quantities, which control the stability of the flow. The critical value of this ratio is known or can be calculated for Newtonian fluid. It is then assumed that this value is the same for all the viscous fluids. Fig. 1 presents the evolution of the critical Reynolds number, Re'_c based on the definition of Metzner and Reed [2], as a function of Hb. A divergence between the different criteria appears when rheological behaviour departs significantly from Newtonian behaviour.

From a theoretical point of view, the main difficulty is to deal with the unyielded plug zone. Nouar and Frigaard [8] perform a non-linear stability analysis of plane Poiseuille

* Corresponding author. Present address: Manchester Center for Nonlinear Dynamics, The University of Manchester, Brunswick Road, Manchester M13 9PL, UK.

E-mail address: jorge@reynolds.ph.man.ac.uk (J. Peixinho).

0377-0257/$ – see front matter © 2005 Elsevier B.V. All rights reserved.
doi:10.1016/j.jnnfm.2005.03.008

Nomenclature

a	dimensionless plug size $\left(= \frac{r_p}{R} = \frac{\tau_Y}{\tau_w}\right)$
B	Bingham number $\left(= \frac{\tau_Y}{K(U/R)}\right)$
E	dimensionless spectrum energy
D	pipe diameter (m)
f	friction factor $\left(= \frac{2\tau_w}{\rho U^2}\right)$
f_N	friction factor for a Newtonian fluid
Hb	Herschel–Bulkley number $\left(= \frac{\tau_Y}{K(U/R)^n}\right)$
k	constant in the Cross model (s)
k'	generalized consistency (Pa $s^{-n'}$)
K	constant in the Herschel–Bulkley model (Pa s^n)
L_e	entrance length (m)
L_p	length between the two pressure tappings (m)
m	power law exponent in the Cross model
n	power law exponent in the Oswald and Herschel–Bulkley
n'	generalized index flow behavior
p	pressure (Pa)
r	radial location within pipe (m)
r_p	radius of constant velocity plastic plug (m)
R	pipe radius (m)
Re	Reynolds number for Newtonian fluid
Re_c	critical Reynolds number for Newtonian fluid
Re'	generalized Reynolds number $\left(= \frac{\rho U^{2-n'} R^{n'}}{8^{n'-1} k'}\right)$
Re'_c	critical generalized Reynolds number
Re_g	Reynolds number $\left(= \frac{\rho U^{2-n'} R^{n'}}{K}\right)$
Re_w	wall Reynolds number $\left(= \frac{\rho U D}{\mu_w}\right)$
t	time (s)
u	axial velocity (m/s)
u'	axial velocity fluctuation (m/s)
u'_c	centreline axial velocity fluctuation (m/s)
u_c	centreline axial velocity (m/s)
u_τ	friction velocity $\left(= \sqrt{\frac{\tau_w}{\rho}}\right)$
u^+	dimensionless velocity $\left(= \frac{u}{u_\tau}\right)$
U	bulk velocity (m/s)
y	distance from the wall (m)
y_τ	friction distance from the wall $\left(= \frac{\mu_w}{\rho u_\tau}\right)$
y^+	dimensionless distance from the wall $\left(= \frac{y}{y_\tau}\right)$
y_c^+	centreline dimensionless distance from the wall
z	longitudinal coordinate (m)

Greek letters

$\dot\gamma$	shear rate (s^{-1})
μ	fluid viscosity (kg m^{-1} s^{-1})
μ_0	zero shear stress dynamic viscosity in the Cross model (kg m^{-1} s^{-1})
μ_w	dynamic viscosity of the fluid at pipe wall (kg m^{-1} s^{-1})
μ_∞	infinite dynamic viscosity in the Cross model (kg m^{-1} s^{-1})
ρ	fluid density (kg m^{-3})
τ	shear stress (Pa)
τ_Y	yield stress (Pa)
τ_w	wall shear stress (Pa)

flow and Hagen–Poiseuille flow of a Bingham fluid, using the energy method, bounds for non-linear stability are derived. Although very weak, these bounds provide a first rigorous demonstration that the Poiseuille flow of a Bingham fluid is more stable than its Newtonian counterpart. Frigaard et al. [9] perform a linear stability analysis of plane Poiseuille flow of a Bingham fluid via Orr–Sommerfeld equations. The numerical results show that the critical Reynolds number based on the plastic viscosity increase with increasing B and $Re_c(B)$ is practically linear for large B. Comparing, the theoretical bounds (linear and non-linear) with the phenomenological criteria shows that only Hanks criterion [3] is compatible with the theoretical bounds for large B. However, for low values of B (the most practical application) it is not possible to determine theoretically which of them is the best criterion. In this situation, the only way to determine, which criteria is most

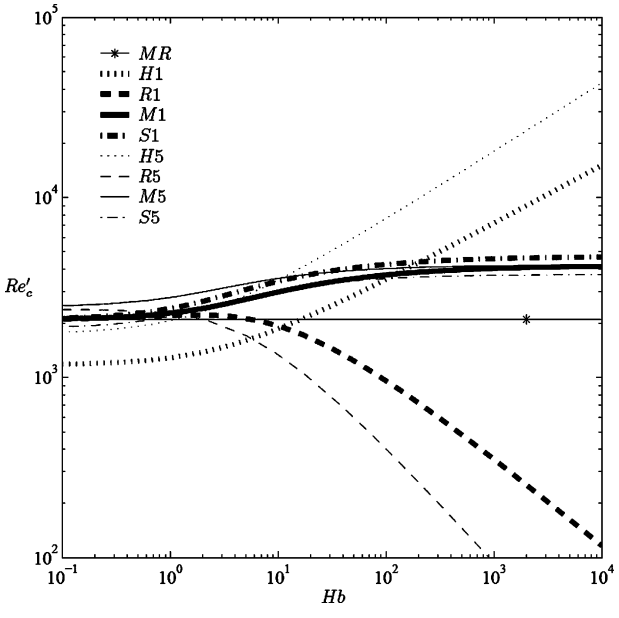

Fig. 1. Critical Reynolds number as a function of the Herschel–Bulkley number: comparison between different criteria—'MR' Metzner and Reed criterion [2]; 'H' Hedström criterion [4], 'R' Ryan and Johnson [5] or Hanks criterion [3]; 'M' Mishra criterion [6]; 'S' Slatter criterion [7]. '5' and '1' indicate $n = 0.5$ and $n = 1$, respectively (n is the power law index of the Herschel–Bulkley model).

applicable is to compare with experimental results. In addition, the linear and non-linear stability analyses for Bingham fluid give little insight into the actual transition mechanisms.

From an experimental point of view, the process whereby turbulence arises is still not understood. The transition is very sensitive on the inlet conditions. Indeed, careful conditions can permit laminar flow for very large Reynolds numbers. Using careful entrance conditions (a settling chamber and a smooth contraction at the entrance of the pipe) and Newtonian (water) and non-Newtonian fluids (dilute polymer solution), Draad et al. [10] produce some finite amplitude stability curves such that impulsive controlled disturbances larger than the threshold produce turbulence, while smaller ones decay downstream. Most of the studies (including the present one) use facilities such that the transition is triggered by intrinsic imperfections of the setup. However Draad et al. or Escudier et al. [11] both observed the transition is delayed in the same trend with the elasticity of the polymer solutions used. To our knowledge, the only experimental results for yield stress fluids are those obtained by Park et al. [12] and Escudier and Presti [13]. Park et al. determine the critical conditions from the pressure drop, the centreline velocity and the corresponding fluctuations. The fluid used is a transparent slurry, which the rheological behaviour is described by a Herschel–Bulkley model ($\tau_Y = 10$ Pa, $K = 0.167$ Pa s^n, and $n = 0.63$). Their results are presented versus Newtonian wall shear rate ($8U/D$), where U is the bulk velocity and D is the diameter of the pipe. It seems that the critical conditions are approximately the same from the different measurements. Using their data, we find $Re'_c = 3500$. Escudier and Presti [13] also measure pressure drop and velocity for a Laponite suspension flow in a pipe. This fluid is thixotropic and the equilibrium curve is described by a Herschel–Bulkley model ($\tau_Y = 4.4$ Pa, $K = 0.24$ Pa s^n, and $n = 0.535$). At sufficiently large Reynolds number, an unexpected result is obtained. In fact, for $900 < Re' < 1400$ (calculated from their data), the velocity profile becomes increasingly asymmetric, although with a well defined plug zone: $r_p = 0.38R$ at $Re' = 1400$. According to Escudier and Presti, this asymmetry could be associated with a minor geometrical imperfection in the flow loop. Then, at $Re' = 2100$, the velocity profile becomes practically symmetrical with a degree of scatter associated with the intense velocity fluctuations, typical for the transition. It is also interesting to note that there is no evidence of a plug zone. Unfortunately, there is no indication how the plug zone evolves when Re' is increased from 1400 to 2100.

For fully developed turbulent flow, Park et al. [12] (suspension of silica particles in oil) and Escudier and Presti [13] (Laponite suspension) observe that the mean velocity profile, as well as the corresponding axial turbulent intensity profile are similar to those obtained for a Newtonian fluid. However, far from the axis, Park et al. find that the axial velocity fluctuations are higher for the slurry than for the Newtonian fluid, whereas Escudier and Presti do not observe a significant difference.

It is clear from this brief literature review, that additional experimental data are needed to understand the influence of the rheological parameters on the transition from laminar to turbulent flow. This is the main objective of the work described here, which is organised as follow. The experimental facility is described in Section 2 together with the instrumentation. Three fluids are used (a yield stress non-thixotropic polymer solution, a shear thinning polymer solution and a Newtonian fluid). Their rheological behaviours are given in Section 3. The measurements performed concern the pressure drop, the time averaged axial velocity profile and the velocity fluctuation profile. Results given in Section 4 show that (i) the shear thinning solution and the yield stress solution stabilize the flow; (ii) the plug zone did not disappear abruptly at the beginning of the laminar to turbulent transition and (iii) the yield stress has no significant effect in the turbulent regime. In Section 5, we summarize our results and make some concluding remarks.

2. Experimental setup and instrumentation

To carry out detailed and reliable velocity and pressure drop measurements, a flow loop is designed. A schematic diagramm is shown in Fig. 2. Flow is provided by an eccentric rotor pump (PCM Moineau) (3) from a 150 l capacity tank (1). The pump flow rate can be set between 20 and 450 l min^{-1}. At the inlet of the test section, a grid (7) prevents any swirl flow, favouring homogeneous turbulence. A 50 l pressurized tank (6) and anti-vibration coupler (2), located after the pump outlet, act to reduce pulsations in the fluid flow before the entrance of the test section (8). The latter is an assembled plexiglas tube of 5.5 m length and 30 mm inside diameter.

A K thermocouple located in the supply tank is used to monitor the fluid temperature. The temperature of the test fluid is controlled by a tubular heat exchanger (CIAT) (4) with an accuracy of 0.2 °C. An electromagnetic flowmeter (Endress + Hauser) (11) operates at the end of the test section (8). For a given flowrate, the total error upon the mean velocity (taking into account the variability of the pump, the flowmeter error and the diameter error) is estimated as 2–3%. Two pressure tappings of 4 mm internal diameter (9) are located at 3.9 and 5.1 m from the inlet of the test section. The tappings are connected to cylindrical chambers, then to tubings that are filled with de-ionised water and finally to the pressure transducer (Druck). The accuracy of the transducer is estimated to be better than 0.25% of the full range of measurement (0–10 mbar). This apparatus improves the pressure measurement making the total error about 1%.

The velocity measurements are made using a laser Doppler anemometer (LDA Dantec FlowLite) system (10). The probe is perpendicular to the test section (8). The axial velocity profile is measured in the horizontal plane at 4.5 m from the inlet of the test section. The probe is mounted on one-axe traverse allowing a radial displacement with spatial resolution of 10 μm. This system comprises a 10 mW helium–neon

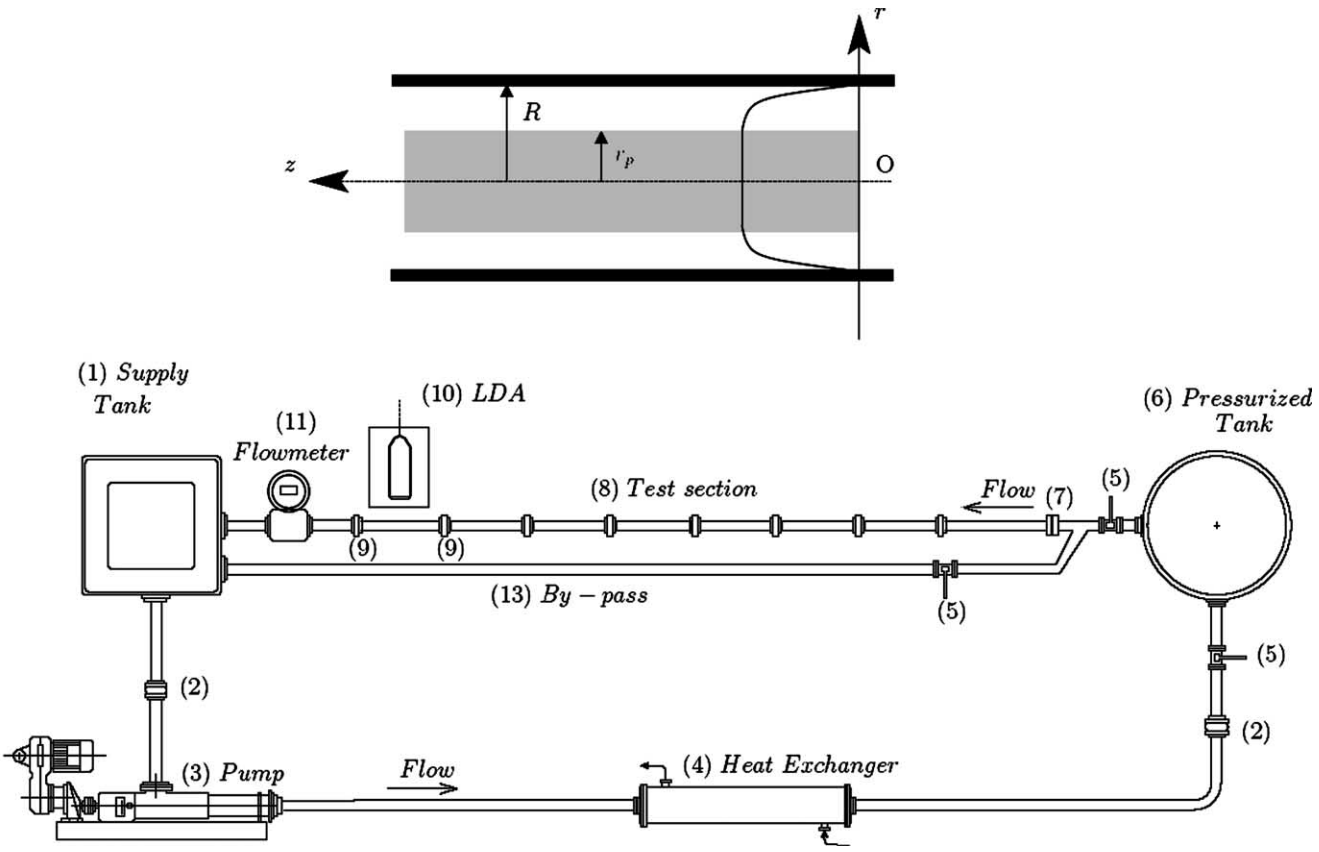

Fig. 2. Schematic diagram of the pipe-flow facility and velocity profile.

(wavelength 632.8 nm) light source, with a (Dantec 57N11 Enhanced) Burst System Analyser processor and a microcomputer (with the BSA Flow Software 1.4). The LDA optical arrangement is characterized by a beam separation at the front lens of 38.4 mm and a focal length of 80 or 160 mm depending on the lens used. The first one (80 mm) is particularly dedicated to near wall measurements. It yields an ellipsoidal measuring volume with a length of principal axis of 166 μm and a diameter of 39 μm. For the second lens (160 mm) the measuring volume length is 651 μm and the diameter is 77 μm. The measurement of the velocity fluctuations are corrected for mean broadening effect according to Durst et al. [14]. In order to improve the signal velocity, flows are seeded with silver coated hollow glass spheres (mean diameter 10 μm). The valid data rates during the experiments were typically 100–1000 Hz. A range of eight times the rms (root mean square) value was arbitrarily selected to obtain a sufficient reliability and to eliminate spurious data without changing the shape of the probability density distribution. Mean velocity and velocity fluctuation are systematically extracted from samples sizes of 40,000 data points. The total uncertainty in the mean velocity is estimated to be in the range 3–4% and in the range 5–6% for the turbulence intensities. The spectrum analysis of the fluctuating velocities was performed with a mean sampling rate of 600 Hz and a measurement time of 1200 s. Each power spectrum is averaged using a fast Fourier transform with 2^{16} points. All the spectra are normalized (such that the area under the spectra are equal) and are plotted versus wavenumber. Preliminary measurements in laminar flow allows estimation of noise level due to the LDA system itself and the imperfections in the flow loop.

As far as the rheological characteristics of the tested fluids are concerned, they are determined using a thermo-regulated controlled stress rheometer (AR2000 from TA Instruments) with a steel 0.5 ° cone/40 mm plate and truncation of 15 μm.

3. Tested fluids

Three types of fluids have been used: (i) a yield stress fluid, (ii) a shear thinning fluid and (iii) a Newtonian fluid as a reference fluid.

3.1. The fluids

- aqueous solutions of 0.2 wt.% Carbopol 940 from B.F. Goodrich.
- aqueous solutions of 2 wt.% sodium CarboxyMethylCellulose 7M1C (CMC) from Hercules Aqualon.
- glucose syrup from Cerestar.

These fluids are used because they are optically transparent, non-toxic and stable (even at relatively high con-

centrations), thereby facilitating LDA measurements. Aqueous solutions of Carbopol and CMC are prepared by adding powder into de-ionised water. Then, the Carbopol solution is neutralized using sodium chloride. A gelification process accompanies this neutralization. To prevent bacteriological degradation of the fluids, a small amount of formaldehyde is added.

3.2. Rheological properties

Fig. 3 shows the variation of shear viscosity vs. shear rate for the 0.2% Carbopol, the 2% CMC and the glucose syrup. The rheograms are determined at the working temperature (20 °C). The experimental data for the 0.2% Carbopol are fitted by the Herschel–Bulkley model according to Roberts and Barnes [15] and Kim et al. [16]. The rheological tests were performed for a shear rate range similar to that encountered in the pipe flow (0.1–4000 s^{-1}). One has to note that the yield stress τ_Y is no more than a fitting parameter, sensible to the resolution of the instrumentation at very low shear rates (some readers prefer the term apparent yield stress). For the 2% CMC solution, three regions can be distinguished depending on the shear rate: (i) a Newtonian region for low shear rate, (ii) a transition region and (iii) a shear thinning region for high shear rate, which can be described by an Ostwald model. For the whole range of shear rate, according to Escudier et al. [17], the rheological behaviour can be well described by the Cross model: $\mu = \mu_\infty + (\mu_0 - \mu_\infty)[1 + (k\dot{\gamma})^m]^{-1}$. On choosing this fluid, we have in mind the regularized models of viscoplastic fluids where the unsheared zone is replaced by highly viscous Newtonian fluid. Due to the mechanical degradation of the fluids particularly at high flow rate, the rheological parameters are determined before and after each experimental test, each reported experiment is associated with the corresponding rheology.

Fig. 4 presents measurement of the first normal stress difference N_1 as a function of the applied shear stress. According to Barnes et al. [18] it can be considered that a liquid is elastic when N_1 in a shear flow is larger than the shear stress. A power law fit to $N_1(\tau)$ data leads to $N_1 = 0.163\tau^{1.41}$ for the 2% CMC solution and $N_1 = 0.085\tau^{1.63}$ for the 0.2% Carbopol solution. Using Barnes criteria the 2% CMC solution and the 0.2% Carbopol solution can be considered highly elastic from $\tau > 90$ Pa and $\tau > 110$ Pa, respectively. These values of shear stress are not achieved before reaching a fully developed turbulent flow (e.g. $Re' > 4000$).

In summary, the flow curves of the 0.2% Carbopol and the 2% CMC are well described by the Herschel–Bulkley and the Cross model, respectively. At high shear rate, both fluids have a similar shear thinning behaviour. According to the first normal stress difference, both aqueous solutions also exhibit similar elastic properties. Consequently, during the flow in a pipe, the only difference between the two solutions is the existence of a plug region.

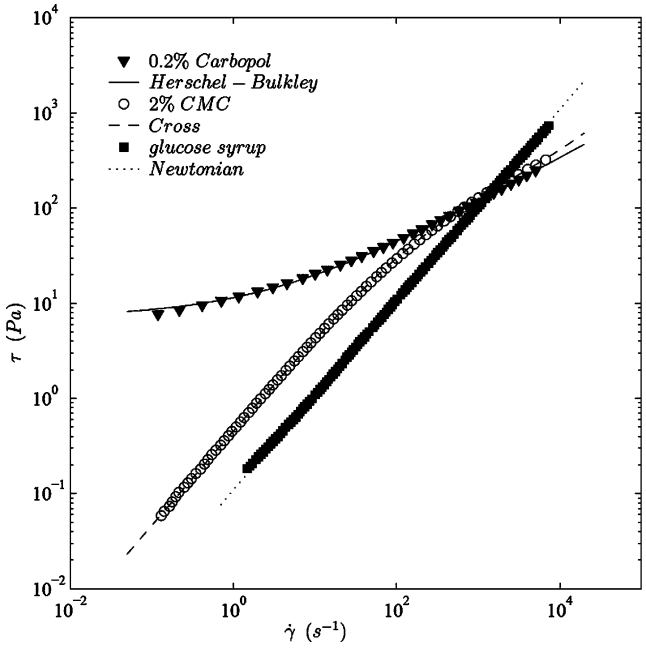

Fig. 3. Shear stress vs. shear rate. The viscosity of the glucose syrup is $\mu = 0.1$ Pa s. The behaviour of the 2% CMC solution is described by the Cross model ($\mu_0 = 0.46$ Pa s, $\mu_\infty = 13.6$ mPa s, $k = 4.75$ ms, $m = 0.71$) and the 0.2% Carbopol solution by the Herschel–Bulkley model (with $\tau_Y = 7.2$ Pa, $K = 4.3$ Pa s^n and $n = 0.47$).

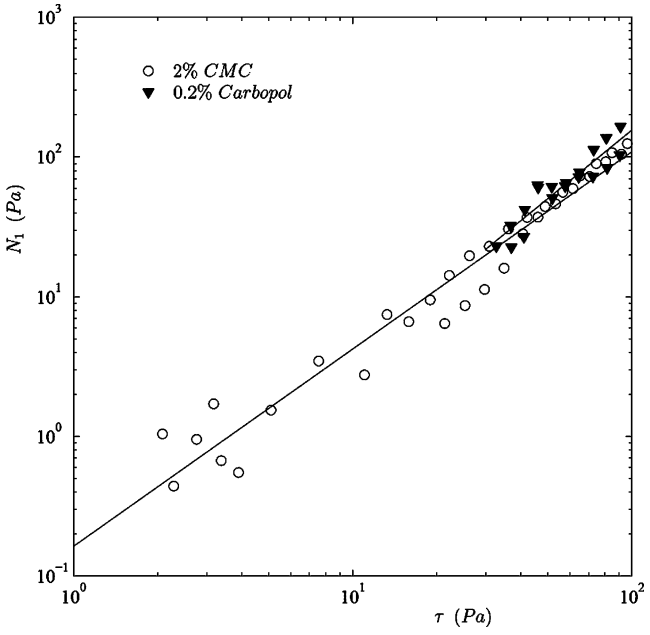

Fig. 4. First normal stress difference vs. shear stress. The lines are power law models: $N_1 = 0.16\tau^{1.4}$ and $0.08\tau^{1.6}$, respectively for the 0.2% Carbopol and the 2% CMC solutions.

4. Results and discussion

The results are presented in three parts. The first one is dedicated to the laminar flow and the validation of our measurements. The second part is dedicated to the transitional flow and the last one to the turbulent flow.

4.1. Laminar flow

According to Froishteter and Vinogradov [19], the entrance length, L_e, after which the laminar flow of a Herschel–Bulkley fluid is considered established is given by:

$$\frac{L_e}{RRe_g} = \frac{0.23}{n^{0.31}} - 0.4a \tag{1}$$

where a is the dimensionless radius of the plug zone, $r_p = aR$ and Re_g is the Reynolds number defined by: $Re_g = \rho U^{2-n} R^n / K$. The Eq. (1) is used to ensure that our measurements concern a fully developed flow.

The Hagen–Poiseuille flow of a Herschel–Bulkley fluid in a cylindrical pipe of radius R is described by:

$$0 = -\frac{dp}{dz} + \frac{1}{r}\frac{d}{dr}(r\tau) \tag{2}$$

where τ is given by:

$$\begin{aligned} \tau &= \mathrm{sgn}\left(\frac{du}{dr}\right)\tau_Y + K\left|\frac{du}{dr}\right|^{n-1}\frac{du}{dr} && |\tau| \geq \tau_Y \\ \frac{du}{dr} &= 0 && |\tau| \leq \tau_Y \end{aligned} \tag{3}$$

where, sgn (du/dr) is the sign of (du/dr), τ_Y the yield stress, K the consistency, and n the flow behaviour index. Using the radius R of the cylinder as length scale and the bulk velocity, U, as velocity scale, the dimensionless solution is:

$$\frac{u}{U} = \begin{cases} \frac{n}{n+1}\left(\frac{Hb}{a}\right)^{1/n}(1-a)^{(n+1)/n} & 0 \leq \frac{r}{R} < a \\ \frac{n}{n+1}\left(\frac{Hb}{a}\right)^{1/n}\left[(1-a)^{(n+1)/n} - \left(\frac{r}{R}-a\right)^{(n+1)/n}\right] & a \leq \frac{r}{R} \leq 1 \end{cases} \tag{4}$$

where Hb is the Herschel–Bulkley number (the ratio of the yield stress τ_Y to a nominal shear stress $K(U/R)^n$). Using the global continuity equation:

$$\int_0^1 \frac{u}{U}\frac{r}{R}\mathrm{d}\left(\frac{r}{R}\right) = \frac{1}{2} \tag{5}$$

It can be shown that:

$$\begin{aligned} 0 = {} & (1-a)^{(3n+1)/n} - \frac{3n+1}{n}(1-a)^{(2n+1)/n} \\ & + \frac{(2n+1)(3n+1)}{2n^2}(1-a)^{(n+1)/n} \\ & + \frac{(3n+1)(2n+1)(n+1)}{2n^3}\left(\frac{a}{Hb}\right)^{1/n} \end{aligned} \tag{6}$$

This equation is solved numerically using Newton's method. The asymptotic behaviour of a as $Hb \to 0$ or $Hb \to \infty$ are:

$$\begin{aligned} a &\sim \left(\tfrac{n}{3+n}\right)^n Hb - \tfrac{1}{2n+1}\left(\tfrac{n}{3+n}\right)^{2n-1} Hb^2 && \text{as} \quad Hb \to 0 \\ a &\sim 1 - c_1\left(\tfrac{1}{Hb}\right)^{1/(1+n)} + c_2\left(\tfrac{1}{Hb}\right)^{2/(1+n)} && \text{as} \quad Hb \to \infty \end{aligned} \tag{7}$$

with, $c_1 = \left(\frac{1+n}{n}\right)^{n/(n+1)}$ and $c_2 = \frac{2n^2}{(2n+1)(n+1)}c_1^2$

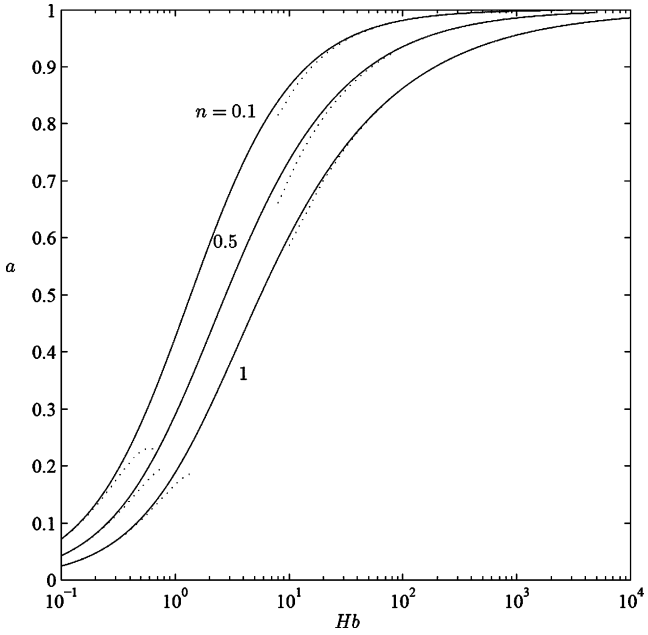

Fig. 5. Dimensionless radius of the plug zone as a function of the Herschel–Bulkley number for $n = 0.1$, 0.5 and 1.

Fig. 5 shows a as a function of Hb for three values of n: 1, 0.5 and 0.1. The dashed lines show the asymptotic expansions to a(Hb) valid for large and small Hb.

Fig. 6 is an example of measured velocity profiles for glucose syrup, 2% CMC solution and 0.2% Carbopol solution in the laminar situation. For the yield stress fluid, the plug zone is delimited by vertical lines. For the corresponding rheology, Eq. (6) gives $a = 0.17$. For the shear thinning fluid the velocity profile is determined numerically. Finally, the experimental velocity profiles are in good agreement with the theoretical ones (continuous, dashed and dotted lines) for the three fluids. The maximum difference between measured and calculated axial velocity does not exceed 2%. These results validate our velocity and rheological measurements.

In the following, the Reynolds number used is that defined by Metzner and Reed [2]. In the laminar regime, it satisfies the relation $fRe' = 16$, were f is the Fanning friction factor. It can be shown that:

$$Re' = \frac{\rho U^{2-n'} D^{n'}}{8^{n'-1}k'} \tag{8}$$

$$n' = \frac{\begin{array}{c}(1-a) + 2a(1-a)(1+m)/(2+m) \\ +(1-a)^2(1+m)/(3+m)\end{array}}{\begin{array}{c}m+1-3(1-a)[a^2 + 2a(1-a)(1+m)/(2+m) \\ +(1-a)^2(1+m)/(3+m)]\end{array}} \tag{9}$$

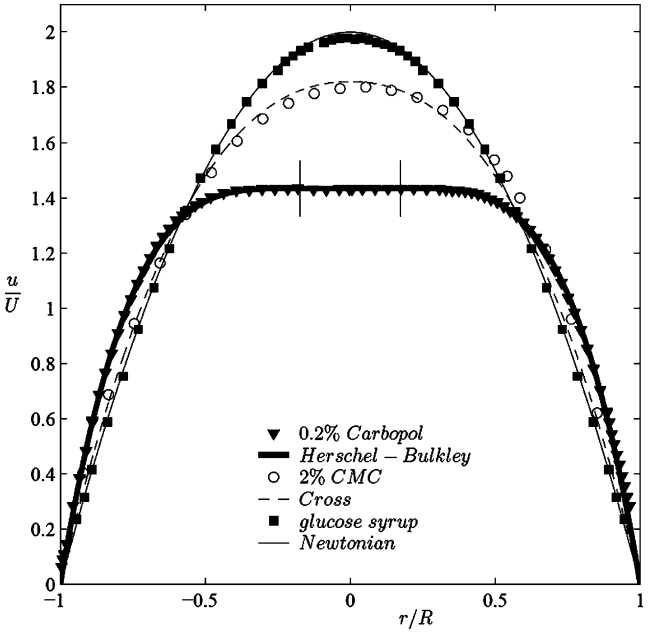

Fig. 6. Laminar velocity profiles for a glucose syrup ($\mu = 0.1$ Pa s, $U = 2.1\,\mathrm{ms}^{-1}$ and $Re = 640$), a 2% CMC ($\mu_0 = 0.17$ Pa s, $\mu_\infty = 0.03$ Pa s, $k = 2.24$ ms, $m = 0.96$, $U = 4.7\,\mathrm{ms}^{-1}$, and $Re' = 1200$) and a 0.2% Carbopol solution ($\tau_Y = 46$ Pa, $K = 15\,\mathrm{Pa\,s}^{-n}$, $n = 0.38$, $U = 3\,\mathrm{ms}^{-1}$, $Hb = 0.42$ and $Re' = 280$).

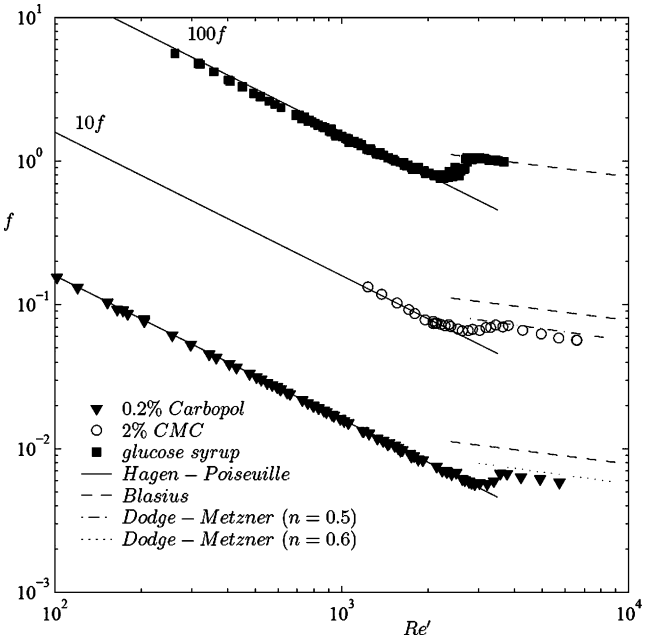

Fig. 7. Friction factor f vs. Reynolds number Re'. The viscosity of the glucose syrup is $\mu = 50$ mPa s. The behaviour of the 2% CMC solution is described by the Cross model ($\mu_0 = 67.1$ mPa s, $\mu_\infty = 4.28$ mPa s, $k = 1.12$ ms, $m = 0.68$) and the 0.2% Carbopol solution by the Herschel–Bulkley model (with $\tau_Y = 6.3$ Pa, $K = 2.2\,\mathrm{Pa\,s}^n$ and $n = 0.5$).

$$k' = \left(\frac{K^m}{4}\right)^{n'} \left(\frac{\tau_Y}{a}\right)^{1-n'm} \left\{(1-a)^{1+m} \times \left[1 + \frac{2(1-a)(1+m)}{a(2+m)} + \frac{(1-a)^2(m+1)}{a^2(3+m)}\right]\right\}^{-n'} \tag{10}$$

where $m = 1/n$. Expressions for n' and k' depend on the Herschel–Bulkley model parameters and the radius of the plug a (obtained by resolving Eq. (6)). Koziki et al. [20] determined n' and k' for several rheological models and ducts arbitrary cross section.

The friction factor f is: $f = \frac{2\tau_w}{\rho U^2}$ with $\tau_w = \frac{R}{2}\frac{\Delta p}{L_p}$, where ρ is the density and Δp a pressure drop over the length L_p between the two pressure tappings along the pipe. The evolution of the friction factor f as a function of Re' is presented in Fig. 7. In the laminar flow situation (e.g. $Re' < 2000$), good agreement is observed between the experimental measurements and the generalized Hagen–Poiseuille law ($fRe' = 16$) for the three fluids used.

Fig. 8 shows the dimensionless centreline velocity u_c/U versus Re', the continuous, dashed and dotted lines represent the theoretical solutions. The ratio u_c/U increases with Re' for the 0.2% Carbopol solution (the plug core dimension decreases) and it decreases with Re' for the 2% CMC solution. Once again the maximum difference between measured and calculated axial velocity does not exceed 2%. All the measurements for laminar flow validate our experimental setup.

4.2. Transitional flow

Fig. 9 illustrates the flow evolution from laminar (a) to turbulent (e) regime for the 0.2% Carbopol solution. With in-

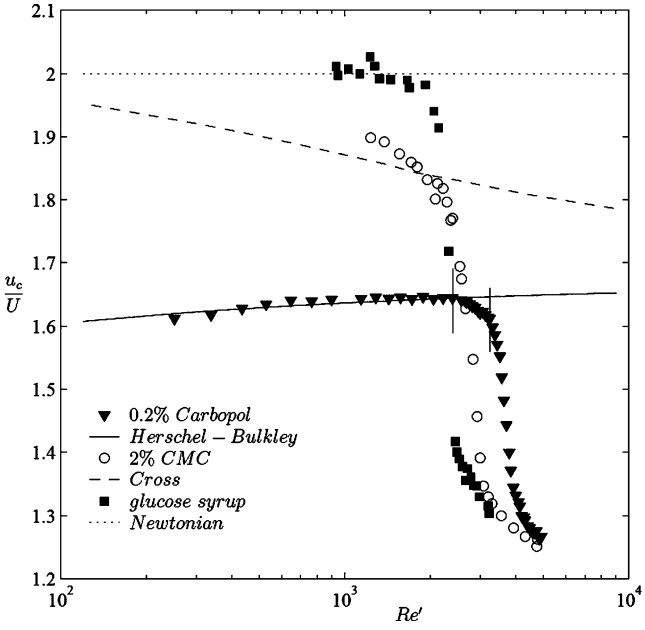

Fig. 8. Normalized centerline velocity u_c/U vs. Re'. The viscosity of the glucose syrup is $\mu = 50$ mPa s. The behaviour of the 2% CMC solution is described by the Cross model ($\mu_0 = 67.1$ mPa s, $\mu_\infty = 4.28$ mPa s, $k = 1.12$ ms, $m = 0.68$) and the 0.2% Carbopol solution by the Herschel–Bulkley model (with $\tau_Y = 2.3$ Pa, $K = 1.9\,\mathrm{Pa\,s}^n$ and $n = 0.5$).

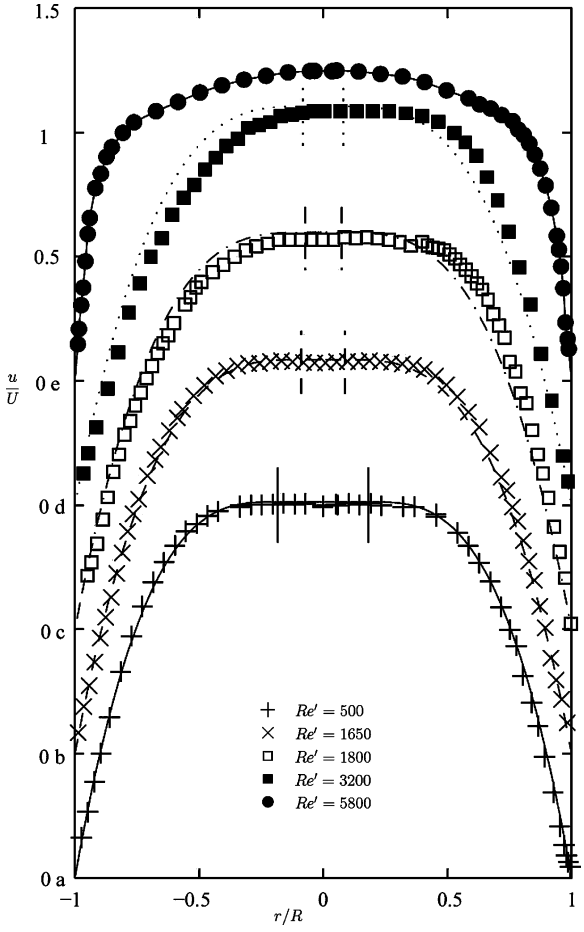

Fig. 9. Mean velocity profiles for increasing Reynolds numbers of 0.2% Carbopol ($\tau_y = 8$ Pa, $K = 2.6$ Pa s^{-n}, $n = 0.49$ and $Hb = 0.182$, 0.088, 0.08 and 0.073, respectively for $Re' = 500$, 1650, 1800 and 3300).

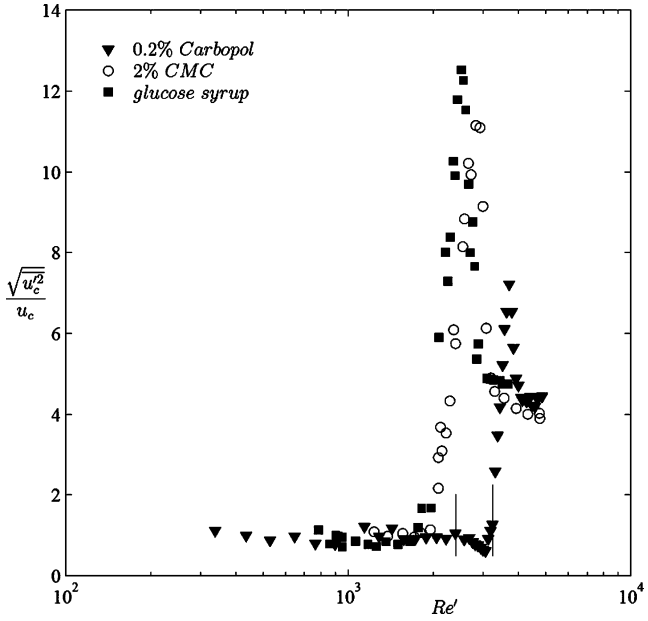

Fig. 10. Relative velocity fluctuations vs. Metzner and Reed Reynolds number. The viscosity of the glucose syrup is $\mu = 50$ mPa s. The behaviour of the 2% CMC solution is described by the Cross model ($\mu_0 = 67.1$ mPa s, $\mu_\infty = 4.28$ mPa s, $k = 1.12$ ms, $m = 0.68$) and the 0.2% Carbopol solution by the Herschel–Bulkley model (with $\tau_Y = 2.3$ Pa, $K = 1.9$ Pa s^n and $n = 0.5$).

creasing the Reynolds number, the experimental velocity profiles (c–d) depart from the corresponding theoretical laminar ones represented by lines. The experimental velocity profile in the transitional regime present an unexpected asymmetry. This repeatable asymmetry also has been observed by Escudier and Presti [13]. It is the object of ongoing investigations.

To determine the critical Reynolds number, the measured centreline velocity is represented as a function of Re' (Fig. 8). At the critical condition, the experimental values start to depart from the theoretical laminar solutions given in the previous section. The same method is used with the friction factor $f(Re')$ (Fig. 7) as well as the centreline velocity fluctuations $\sqrt{u_c'^2}/u_c(Re')$ (Fig. 10). One can note that the mean centreline velocity and the centreline velocity fluctuations are extracted from the same velocity signal. The results are summarized in Table 1. The critical conditions calculated from three different phenomenological criteria are also given for comparison. Mishra and Hanks criteria are the most in agreement with the experimental results. It is clear that the shear thinning and the yield stress delay the transition as observed by Pinho and Whitelaw [21], Park et al. [12] and Escudier and Presti [13]. The results given in Table 1 also show that for fluids without yield stress (i.e. glucose and CMC solutions), the critical Reynolds number evaluated using $\sqrt{u_c'^2}/u_c(Re')$ is lower than that obtained from $u_c/U(Re')$ or $f(Re')$ measurements. The method based on the analysis of the $\sqrt{u_c'^2}/u_c(Re')$ is more sensitive to detect the beginning of the transition than the other two methods. However, for the 0.2% Carbopol

Table 1
Phenomenological and experimental criteria : the glucose syrup is a Newtonian fluid (with a viscosity of 50 mPa s)

Fluids	Experimental criteria			Phenomenological criteria		
	$f(Re')$	$\frac{u_c}{U}(Re')$	$\frac{\sqrt{u_c'^2}}{u_c}(Re')$	Mishra	Hanks	Slatter
Glucose syrup	2100	2050	1800	2100	2100	2100
2% CMC	2500	2300	2100	2230	2268	–
0.2% Carbopol	2700	2550	3300	2485	2380	1907

The behaviour of the 2% CMC solution is described by the Cross model ($\mu_0 = 67.1$ mPa s, $\mu_\infty = 4.28$ mPa s, $k = 1.12$ ms and $m = 0.68$) and the 0.2% Carbopol solution by the Herschel–Bulkley model (with $\tau_Y = 2.3$ Pa, $K = 1.9$ Pa s^n and $n = 0.5$).

solution, Re'_c from $\sqrt{\overline{u'^2_c}}/u_c(Re')$ is larger than Re'_c from $u_c/U(Re')$ or $f(Re')$. This case will be analyzed in detail later.

Concerning the transition, Fig. 8 shows the evolution of $u_c/U(Re')$ for the fluids used. Different stages can be distinguished. For the Newtonian fluid, an abrupt decrease of the ratio u_c/U is observed for $2000 < Re < 3000$. Then, for $Re > 3000$, the ratio is close to values given in the literature by Pinho and Whitelaw [21]. For the 2% CMC solution, the evolution is similar to that for a Newtonian fluid. In the case of the Herschel–Bulkley fluid, the evolution of u_c/U versus Re' can be described in three stages. In the first stage, u_c/U (instead of increasing goes in the opposite direction and) decreases slightly with increasing Re'. In the second stage, an abrupt decrease of u_c/U is observed and in the third stage ($Re' > 4000$), the decrease of u_c/U becomes weaker. The vertical lines represent $Re' = 2550$ and $Re' = 3300$.

From the centreline velocity signal, we can also analyse the evolution of the fluctuations as a function of Re' (Fig. 10). The bounds ($Re' = 2550$ and $Re' = 3300$) given previously are also represented by vertical lines. In the case of the Newtonian fluid, from $Re = 1800$, the relative velocity fluctuation departs from 1% level (due to the imperfections of the experimental setup and the noise level of the LDA system) and increases sharply to the maximum value of 12% at $Re = 2500$. Park et al. [12] find a maximum turbulent intensity of 11% for a glycerine–water mixture. Then, the relative velocity fluctuation decreases rapidly and reaches 5% at $Re = 2800$. A similar evolution is observed for the CMC and the Carbopol solutions, however the maximum are respectively 10% at $Re' = 2900$ and 7% at $Re' = 3700$. Escudier and Presti [13] find a maximum of about 6% and Park et al. [12] a maximum of 5% (for a mixture of Stoddard solvent and mineral oil considered as a Herschel–Bulkley fluid: $\tau_Y = 10$ Pa, $K = 0.17$ Pa s^n, $n = 0.63$ and $Hb = 2.85$). One can note that the peak of relative velocity fluctuation for the yield stress fluid is much lower than for the Newtonian fluid in the transition region. Indeed, the maximum of $\sqrt{\overline{u'^2_c}}/u_c(Re')$ depends on the difference of u_c/U in laminar and u_c/U in turbulent regime. In the case of Herschel–Bulkley fluid, this difference is less pronounced than for Newtonian fluid. Besides, the maximum of the relative velocity fluctuation curve corresponds to the inflection point of the $u_c/U(Re')$ curve. It is also important to remark that for the Carbopol solution the fluctuations remain at a laminar level in the first stage of the transition (between the bounds observed previously: $2550 < Re' < 3300$).

This result can also be observed in Fig. 11. It gives velocity fluctuations profiles normalized by the bulk velocity corresponding to the mean velocity profiles of the Fig. 9. The first two are measured at $Re' = 500$ and 1650. They are very similar and representative of the laminar regime. The noise level is 2% on the axis and increases closer to the wall despite the correction for the mean broadening effect. The third one is obtained at $Re' = 1800$ seems to depart from the laminar profile but remains close to the uncertainty domain. The fourth profile at $Re' = 3200$ is clearly distinguishable from the laminar one. It was obtained in the first step of the transition. Here, once again in the core flow, the fluctuations remain at the same level as in the laminar regime and increase outside this zone. Therefore, the flow can be unstable in the presence of a plug zone. This peculiar, but repeatable profile is not obtained for the Newtonian and the shear thinning fluids. The last profile at $Re' = 5800$ was obtained in fully turbulent flow.

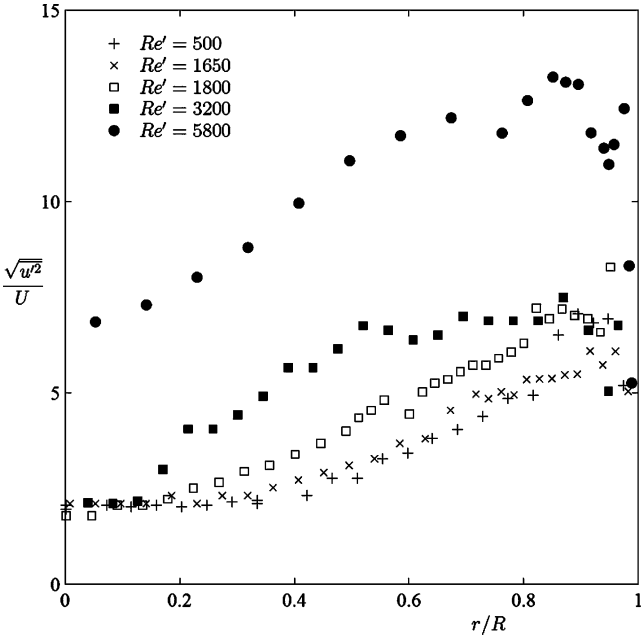

Fig. 11. Relative velocity fluctuations profiles of 0.2% Carbopol ($\tau_Y = 8$ Pa, $K = 2.6$ Pa s^{-n}, $n = 0.49$ and $Hb = 0.182$, 0.088, 0.08 and 0.073, respectively for $Re' = 500$, 1650, 1800 and 3200).

The first stage of transition can also be detected experimentally through the velocity signal given by an oscilloscope. Fig. 12 presents four velocity time history signals at $r/R = 0$ (on the centerline of the pipe) and at $r/R = 0.65$ (where the relative velocity fluctuation increases significantly compared to laminar case) for two different Re' (3200 and 3600). The velocity signal at $r/R = 0$ and $Re' = 3200$ is stable, whereas the velocity at the same Re' but at $r/R = 0.65$ is clearly unstable. For larger Re' (at $Re' = 3600$), the signal shows coexistence of laminar and turbulent zones particularly on the centerline, whereas at $r/R = 0.65$ the signal appears even more complex in the sense that low frequency oscillations and turbulent spots are present. Fig. 13 shows the associated wavenumber normalized power spectra of the fluctuating velocities at $r/R = 0.65$ and $Re' = 2600$, 2700 and 3200. This first stage is called 'low frequency stage'. It may be linked to disturbances having not enough energy to produce a turbulent spot: the range of viscosity can become so large that whereas instabilities can grow in the wall region they are dampened close to the centerline.

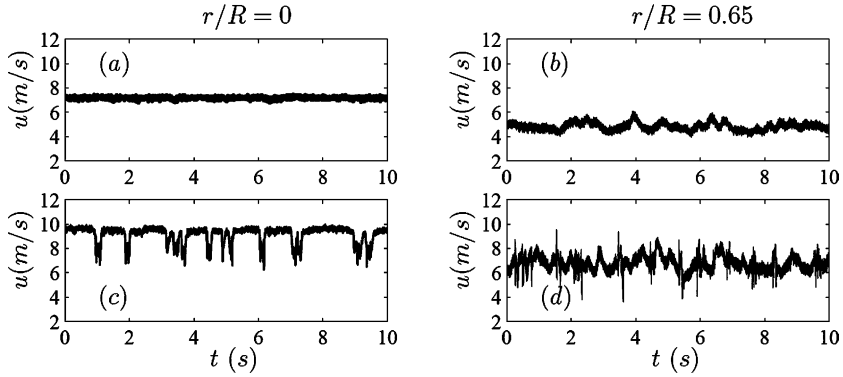

Fig. 12. Velocity time history for a 0.2% Carbopol solution ($\tau_Y = 2.3$ Pa, $K = 10$ Pa s^{-n}, and $n = 0.32$) (*a*) $r/R = 0$ and $Re' = 3200$, (*b*) $r/R = 0.65$ and $Re' = 3200$, (*c*) $r/R = 0$ and $Re' = 3600$ and (*d*) $r/R = 0.65$ and $Re' = 3600$.

During the first stage of the transition, the centreline velocity signal remains similar to that in the laminar regime. In the second stage of the transition, turbulent spots are observed experimentally. Fig. 12(c) is a sample of velocity time history at $Re' = 3600$ on the centerline of the pipe. From this, an isolated turbulent spot in dimensionless form is given by Fig. 14(a). Inside the spot, the plug zone is disrupted due to large velocity variations. In the laminar phase between two spots, the presence of the plug zone is possible. Hence, if the length of the pipe is sufficiently long, a discontinuous plug zone can be observed. Fig. 14 shows typical spots for the CMC solution (Fig. 14(b)), glucose syrup (Fig. 14(c)) and that given by Darbyshire and Mullin [22] for water (Fig. 14(d)). It can be observed that all the spots have practically the same length scale ($\simeq 25D$). The velocity variation between the laminar and turbulent phase depends on the non-Newtonian character of the fluid as explained before. With increasing Re', the continuous development of several turbulent spots leads to completely turbulent flow.

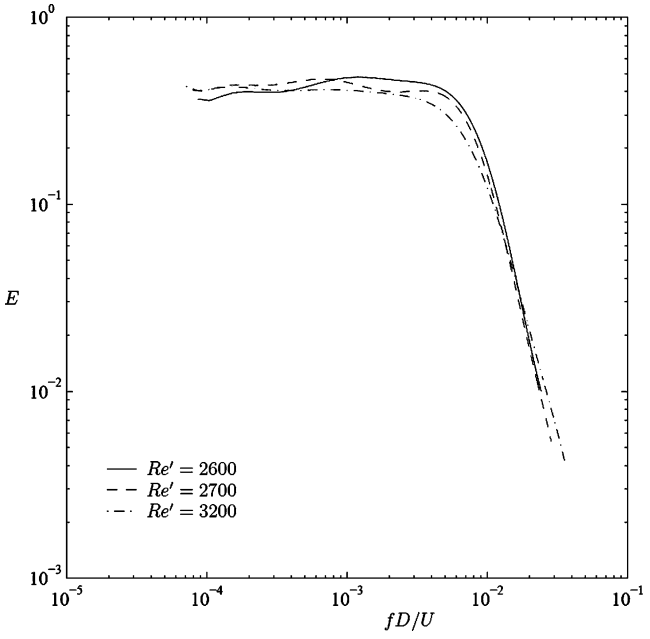

Fig. 13. Normalized power spectra of axial velocity fluctuation of a 0.2% Carbopol solution ($\tau_Y = 2.3$ Pa, $K = 10$ Pa s^{-n}, and $n = 0.32$) at the position $r/R = 0.65$ during the first stage of transition at $Re' = 2600$, 2700 and 3200.

4.3. Turbulent flow

The analysis of the turbulent flow at low Reynolds number for the three fluids considered is made through friction factor measurements as a function of the wall Reynolds number Re_w (based on the wall viscosity). The mean velocity profile and the turbulent intensity profile of the axial velocity are also considered.

4.3.1. Friction factor

The variation of friction factor with Re_w is presented in Fig. 15. The experimental measurements for glucose syrup are in very good agreement with Blasius law for $Re > 3000$. For Carbopol solution, the experimental results are lower than the Dodge and Metzner correlation [23] (represented as dashed lines). Actually, at these Re_w, the elasticity of the fluid leads to the drag reduction effect such that the drag reduction coefficient ($DR = 100(f - f_N)/f_N$ where f_N is the friction factor for a Newtonian fluid) is about 30 and 35% in the range of Re_w tested, respectively for the 0.2% Carbopol solution and the 2% CMC solution.

4.3.2. Mean velocity profile

Velocity profiles are presented in Fig. 16. The centreline of the pipe corresponds to $y_c^+ \approx 144$ for the glucose syrup, $y_c^+ \approx 270$ for the 2% CMC solution and $y_c^+ \approx 283$ for the 0.2% Carbopol solution. For the glucose syrup, the normalized velocity profile agrees with the linear relation: $u^+ = y^+$ for $0 < y^+ < 5$ and the low Reynolds number logarithmic relation: $u^+ = 2.5 \ln y^+ + 5.5$ for $y^+ > 30$ obtained by Patel and Head [24]. Dodge and Metzner [2] and Virk correlations are represented by dashed lines. Velocity measurements show drag reduction effects. It is difficult to conclude upon the in-

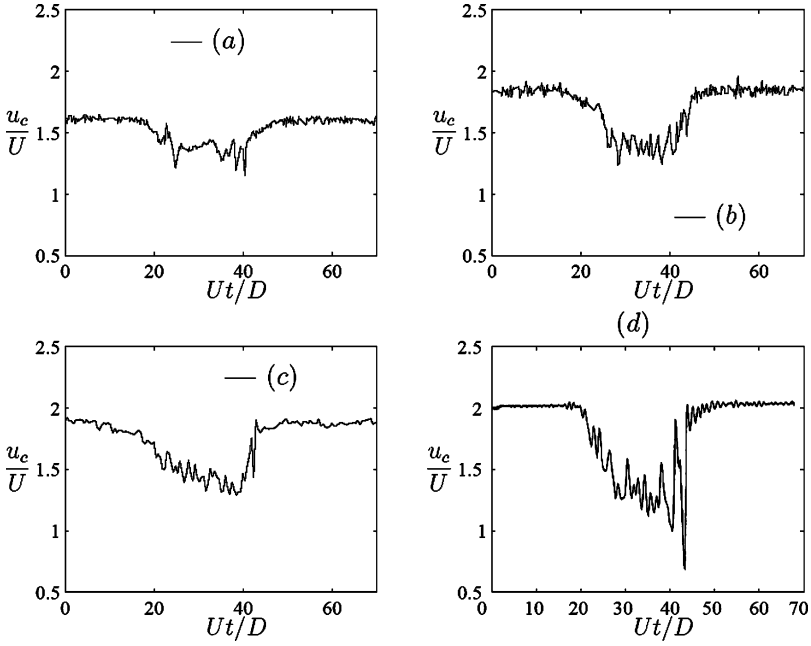

Fig. 14. Time trace of the axial velocity on the centerline of the pipe (*a*) for a 0.2% Carbopol solution ($\tau_Y = 2.3$ Pa, $K = 10$ Pa s^{-n}, $n = 0.32$, and $Re' = 3600$), (*b*) for a 2% CMC solution ($\mu_0 = 67.1$ mPa s, $\mu_\infty = 4.28$ mPa s, $k = 1.12$ ms, $m = 0.68$, and $Re' = 3280$) , (*c*) for a glucose syrup ($\mu = 105$ Pa s, $Re = 2000$), and (*d*) from Darbyshire and Mullin [22] for water (at $Re \simeq 2200$).

fluence of the shear thinning since the elasticity of the fluids is important. Indeed, from pressure measurements (Fig. 15) and first normal stress measurement (Fig. 4), one can estimate the first normal stress is higher than the wall shear stress near the wall.

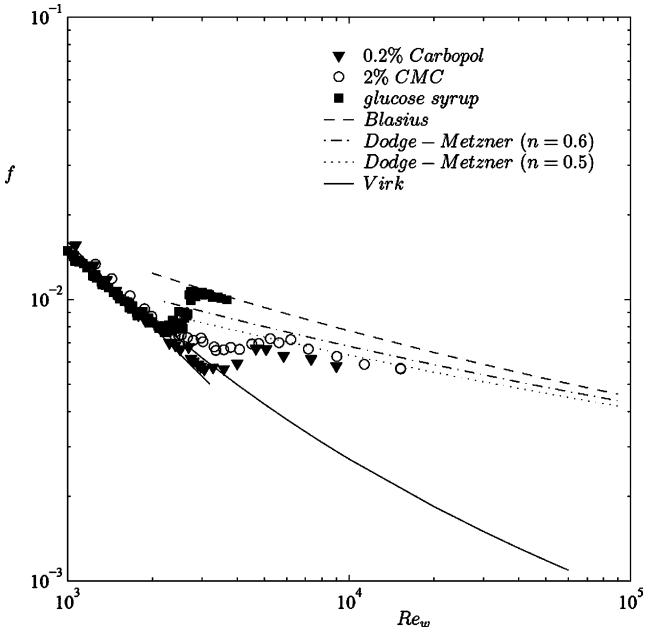

Fig. 15. Friction factor f vs. Reynolds number Re'. The viscosity of the glucose syrup is $\mu = 50$ mPa s. The behaviour of the 2% CMC solution is described by the Cross model ($\mu_0 = 67.1$ mPa s, $\mu_\infty = 4.28$ mPa s, $k = 1.12$ ms and $m = 0.68$) and the 0.2% Carbopol solution by the Herschel–Bulkley model (with $\tau_Y = 6.3$ Pa, $K = 2.2$ Pa s^n and $n = 0.5$).

4.3.3. Turbulent intensity profile

Fig. 17 represents $\sqrt{\overline{u'^2}}/u_\tau$ as a function of y^+. It increases from the wall and reaches a maximum before decreasing. For the glucose syrup, the experimental results are

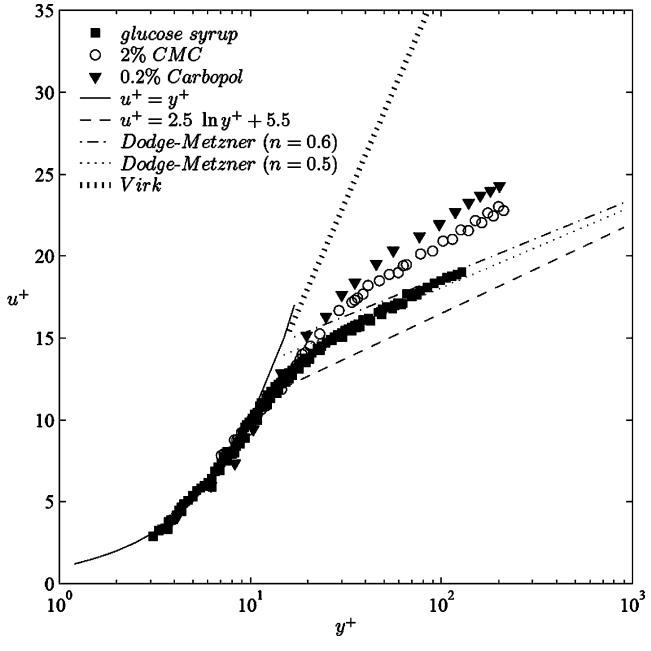

Fig. 16. Mean velocity profile. The viscosity of the glucose syrup is $\mu = 52$ mPa s and $Re = 4000$. The behaviour of the 2% CMC solution is described by the Cross model ($\mu_0 = 67.1$ mPa s, $\mu_\infty = 4.28$ mPa s, $k = 1.12$ ms and $m = 0.68$) and $Re_w = 12000$. The 0.2% Carbopol solution is described by the Herschel–Bulkley model (with $\tau_Y = 5.5$ Pa, $K = 3$ Pa s^{-n} and $n = 0.49$) and $Re_w = 10000$.

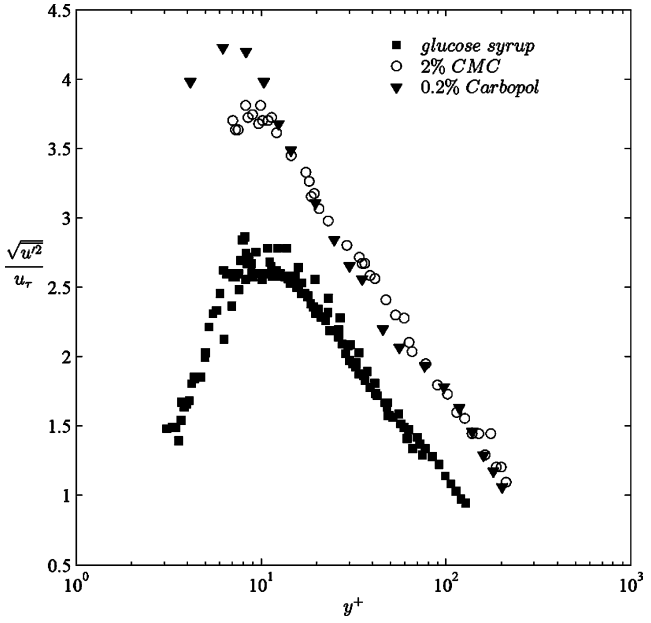

Fig. 17. Turbulent intensity profile. The viscosity of the glucose syrup is $\mu = 52\,\text{mPa s}$ and $Re = 4000$. The behaviour of the 2% CMC solution is described by the Cross model ($\mu_0 = 67.1\,\text{mPa s}$, $\mu_\infty = 4.28\,\text{mPa s}$, $k = 1.12\,\text{ms}$ and $m = 0.68$) and $Re_w = 12000$. The 0.2% Carbopol solution is described by the Herschel–Bulkley model (with $\tau_Y = 5.5\,\text{Pa}$, $K = 3\,\text{Pa s}^{-n}$ and $n = 0.49$) and $Re_w = 10000$.

in a very good agreement with those given by Durst et al. [14], the peak of the turbulence intensity is 2.6 and located at $y^+ \simeq 12$. For the 2% CMC solution and the 0.2% Carbopol solution, the peak is higher than for Newtonian fluid. The measurements of axial velocity for Carbopol and CMC solutions are difficult for $y^+ < 10$ (actually $y^+ = 10$ correspond to $y \approx 0.2\,\text{mm}$). This is why there is a lack of experimental data in Fig. 17 for low y^+. Once again there is a dominant effect of the elasticity of the fluids. Nevertheless, our measurement shows the peak of the axial turbulence intensity is larger than for Newtonian fluids.

5. Conclusion

In this paper, detailed measurements have been carried out in laminar, transitional and turbulent pipe flow of a yield stress fluid (0.2% Carbopol solution), a shear thinning fluid (2% CMC solution) and a Newtonian fluid (glucose syrup). The first normal stress differences are similar for the two non-Newtonian fluids. In laminar flow, the experimental velocity profiles and the friction factor are well described by the theoretical solution. The critical conditions from which the centreline velocity and the pressure drop measurements depart from theoretical solutions are determined. The results show that both the shear thinning and the yield stress increases the stability of the flow. The critical conditions are compared with various phenomenological criteria. It seems that the global stability criterion given by Hanks et al. [3] and Mishra et al. [6] are the most appropriate to predict our results.

The transition for the yield stress fluid takes place in two stages. First, the experimental velocity profile departs slightly from the laminar theoretical solution, however, the fluctuations remain at a laminar level in a zone flow around the axis and increase slightly outside this zone. In the annular zone, low frequency oscillations of the axial velocity are observed. Then, with increasing the Reynolds number, turbulent spots filling up the whole section appear. Inside the spot, the plug zone is disrupted due to large velocity variations. Between two successive spots, the flow is laminar, then the presence of the plug zone is possible.

In turbulent flow, the friction factor measurements and velocity profiles show the drag reduction effect for both the 2% CMC and the 0.2% Carbopol solutions. Near the axis, the longitudinal turbulence intensities are similar to that of Newtonian fluid. However, in the vicinity of the wall, the axial relative turbulence intensities are larger than for Newtonian fluid. This is in agreement with Park et al. [12].

Acknowledgments

The authors would like to thank our colleagues for useful discussion, the management of Schlumberger for financial support and permission to publish this work and M. Belakhar for her assistance in some of the latest experiments.

References

[1] R.B. Bird, G.C. Armstrong, O. Hassager, Dynamics of Polymer Liquids, vol. 1, Wiley, 1977.
[2] A.B. Metzner, J.C. Reed, Flow of non-Newtonian fluids-correlation of laminar, transition and turbulent-flow regions, A.I.Ch.E. J. 1 (1955) 433–435.
[3] R.W. Hanks, The laminar-turbulent transition for fluids with a yield stress, A.I.Ch.E. J. 9 (1963) 306–309.
[4] B.O.A. Hedström, Flow of plastics materials in pipes, Ind. Eng. Chem. 44 (3) (1952) 651–656.
[5] N.W. Ryan, M.M. Johnson, Transition from laminar to turbulent flow in pipes, A.I.Ch.E. J. 5 (1959) 433–435.
[6] P. Mishra, G. Tripathi, Transition from laminar to turbulent flow of purely viscous non-Newtonian fluids in tubes, Chem. Eng. Sci. 26 (1971) 915–921.
[7] P.T. Slatter, The laminar-turbulent transition prediction for non-Newtonian slurries, Proceedings of the International Conference on Problems in Fluid Mechanics and Hydrology, vol. 1, Prague, 1999, pp. 247–256.
[8] C. Nouar, I.A. Frigaard, Non-linear stability of Poiseuille flow of a Bingham fluid: theoretical results and comparison with phenomenological criteria, J. Non-Newtonian Fluid Mech. 100 (2001) 127–149.
[9] I.A. Frigaard, S.D. Howison, I.J. Sobey, On the stability flow of a Bingham fluid, J. Fluid Mech. 263 (1994) 133–150.
[10] A.A. Draad, G.D.C. Kuiken, F.T.M. Nieuwstadt, Laminar-turbulent transition in pipe flow for Newtonian and non-Newtonian fluids, J. Fluid Mech. 377 (1996) 267–312.
[11] M.P. Escudier, F. Presti, S. Smith, Drag reduction in the turbulent pipe flow of polymers, J. Non-Newtonian Fluid Mech. 81 (1999) 197–213.

[12] J.T. Park, R.J. Mannheimer, T.A. Grimley, T.B. Morrow, Pipe flow measurement of a transparent non-Newtonian slurry, J. Fluids Eng. 111 (1989) 331–336.
[13] M.P. Escudier, F. Presti, Pipe flow of a thixotropic liquid, J. Non-Newtonian Fluid Mech. 62 (1996) 291–306.
[14] F. Durst, J. Jovanović, J. Sender, LDA measurements in the near-wall region of a turbulent pipe flow, J. Fluid Mech. 295 (1995) 305–335.
[15] G.P. Roberts, H.A. Barnes, New measurements of the flow-curves for Carbopol dispersions without slip artefacts, Rheol. Acta 40 (2001) 499–503.
[16] J.-Y. Kim, J.-Y. Song, E.-J. Lee, S.-K. Park, Rheological properties and microstructures of Carbopol gel network system, Colloid Polym. Sci. 281 (2003) 614–623.
[17] M.P. Escudier, I.W. Gouldson, A.S. Pereira, F.T. Pinho, R.J. Poole, On the reproducibility of the rheology of shear-thinning liquids, J. Non-Newtonian Fluid Mech. 97 (2001) 99–124.
[18] H.A. Barnes, J.F. Hutton, K. Walters, An introduction to Rheology, Elsevier, 1989.
[19] G.B. Froishteter, G.V. Vinogradov, The laminar flow of plastic disperse systems in circular tubes, Rheol. Acta 19 (1980) 239–250.
[20] W. Kozicki, C.H. Chou, C. Tiu, Non-Newtonian flow in ducts of arbitrary cross-section shape, Chem. Eng. Sci. 21 (1966) 665–679.
[21] F.T. Pinho, J.H. Whitelaw, Flow of non-Newtonian fluids in a pipe, J. Non-Newtonian Fluid Mech. 34 (1990) 129–144.
[22] A.G. Darbyshire, T. Mullin, Transition to turbulence in constant-mass-flux pipe flow, J. Fluid Mech. 289 (1995) 83–114.
[23] D.W. Dodge, A.B. Metzner, Turbulent flow of non-Newtonian systems, A.I.Ch.E. J. 5 (1959) 189–204.
[24] V.C. Patel, M.R. Head, Some observations on skin friction and velocity profiles in fully developed pipe and channel flows, J. Fluid Mech. 38 (1969) 181–201.